Optics Communications 439 (2019) 129–132

Contents lists available at ScienceDirect

Optics Communications

journal homepage: www.elsevier.com/locate/optcom

Astronomical observation by 2-meter telescope based on liquid crystal adaptive optics with phase diversity

Daosheng Wu [a,b], Chengliang Yang [a,*], Hao Li [a,b], Peiguang Zhang [a], Xingyun Zhang [a], Zhaoliang Cao [a], Quanquan Mu [a,*], Li Xuan [a]

[a] State Key Laboratory of Applied Optics, Changchun Institute of Optics, Fine Mechanics and Physics, Chinese Academy of Sciences, Changchun, Jilin, 130033, China
[b] University of Chinese Academy of Sciences, Beijing, 100049, China

ARTICLE INFO

Keywords:
Phase diversity
Image restoration
Liquid crystal
Adaptive optics

ABSTRACT

A set of liquid crystal adaptive optics system for visible light is installed for 2-meter telescope in Changchun, China. To get higher resolution images after adaptive optics, phase diversity (PD) is applied. Two liquid crystal spatial light modulators were used for two polarized states of light, and they were also used for two channel correction of focused image and diversity image. Observations about star HD 29139 were performed on March 23, 2018. The results of the star with the PD show that the full width half maximum was decreased from about 10 pixels to 4 pixels, corresponding to angular resolution improved from 0.5" to 0.2". The peak intensity was improved by 66.7% after the PD. The root mean square of the wavefront estimated using the PD agrees with the Strehl ratio of observed image after adaptive optics. The observed results indicate that the PD technique can significantly improve the image resolution after liquid crystal adaptive optics.

1. Introduction

Adaptive optics (AO) is being used in many large aperture ground-telescopes for astronomical observation [1–4]. We develop a set of liquid crystal AO system (LC AOS) for the 2-m telescope at Changchun Institute of Optics, Fine Mechanics and Physics, Chinese Academy of Sciences. However, it is difficult to attain full compensation especially for visible wavelengths. To improve image resolution after AO, some image processing algorithms need be used [5–7]. Compared to other methods, phase diversity (PD) can restore the point source as well as extended objects and has a simple and easy-to-achieve optical layout. Thus we apply the PD to improve the image quality.

The PD was firstly proposed by Gonsalves in 1979 [8]. This technique uses a focused image and one or more images with known phase diversity to reconstruct the wavefront and restore the image. In 1994, the PD technique was applied to solar imaging system successfully [9,10]. It improved the image resolution effectively by estimating the aberrations resulting from atmospheric turbulence. In 2008, Mugnier et al. proposed long-exposure PD technique which allows the PD technique can be used for the long exposure AO corrected images for quasi-static aberrations sensing and high-resolution image reconstructing [11]. After decades of development, PD is no longer used just for AO wavefront sensing and image post-processing [12,13], but also for optical misalignment sensing in segmented aperture telescopes [14], sensing of non-common path aberrations in AO systems [15], and complex magnitude sensing of lasers [16].

Liquid crystal spatial light modulators (LC SLMs) are widely used in light field regulation [17] and has high pixel density, so it can easily meet the demand for large actuator number for adaptive optics with large aperture telescope. LC AOS has been deeply studied and achieved a series of developments [18–20]. In 2002, Air Force Research Laboratory introduced dual-frequency liquid crystal to astronomical adaptive optics system and applied it on the AEOS 3.67-m telescope [21]. In 2012, Z. Cao et al. performed an open-loop liquid crystal adaptive optics correction experiment on a 1.2-m telescope [22]. A star with a visual magnitude of 4.45 was corrected and 0.31″ angular resolution was achieved. In 2017, Z. Xu et al. applied PD technique to open loop LC AOS, and improved the image resolution of optical USAF-1951 resolution test chart in the laboratory [23].

In this work, the PD technique is applied to LC AOS for 2-m telescope in Changchun, China, where the atmosphere coherence length was about 5 cm. The observation about single star HD 29139 was performed on March 23, 2018. The experimental results after the PD show that full width half maximum (FWHM) of the star decreased from 10 pixels to 4 pixels, and the angular resolution correspondingly was improved from 0.5″ to 0.2″. The peak intensity was also improved. The root mean square (RMS) of the wavefront estimated using the PD agrees with the Strehl ratio (SR) of AO corrected image. The results indicate that the PD technique can significantly improve the image resolution after LC AOS.

* Corresponding authors.
E-mail address: ycldahai@ciomp.ac.cn (C. Yang).

https://doi.org/10.1016/j.optcom.2019.01.036
Received 4 September 2018; Received in revised form 7 January 2019; Accepted 13 January 2019
Available online 17 January 2019

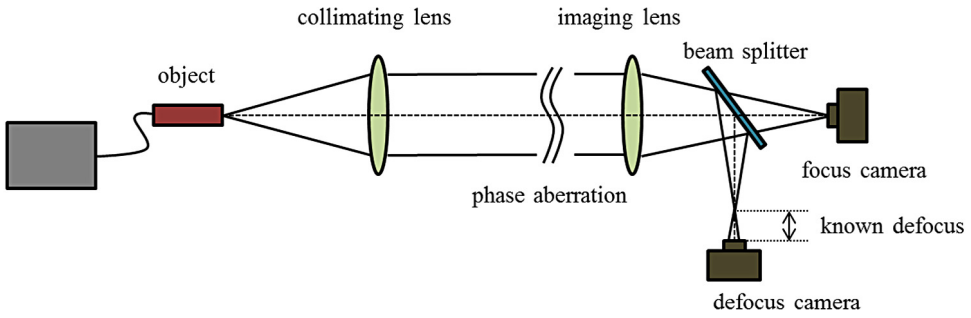

Fig. 1. Optical setup of classic phase diversity technique.

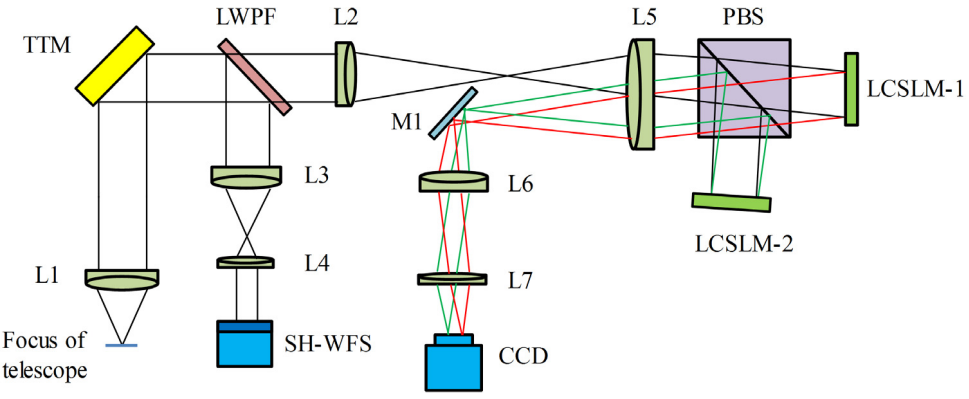

Fig. 2. The optical layout of LC AOS. L1, L2, L3, L4, L5, L6, L7 are lenses, TTM is tip/tilt mirror, LWPF is long wavelength pass filter, SH-WFS is Shack–Hartmann wavefront sensor, PBS is polarized beam splitter, M1 is mirror.

2. PD theory

The PD technique needs a focused image and an image with known phase diversity. For brevity, diversity phase is defocus in the following discussion. This PD can be done with simple optical setup as shown in Fig. 1.

The focused image can be modeled as Eq. (1):

$$g(\mathbf{x}) = f(\mathbf{x}) * h(\mathbf{x}) + n(\mathbf{x}), \tag{1}$$

where * stands for spatial convolution, $g(\mathbf{x})$ is the focused image, $\mathbf{x}$ are two-dimensional spatial coordinates, $f(\mathbf{x})$ is the original object, $n(\mathbf{x})$ is the additive noise, $h(\mathbf{x})$ is the point spread function, which includes aberrations not only from optical systems, but also from propagation medium, especially for atmosphere turbulence. $h(\mathbf{x})$ can be written as:

$$h(\mathbf{x}) = |FT(P(\mathbf{x})\exp(i\phi(\mathbf{x})))|^2, \tag{2}$$

where $P(\mathbf{x})$ is the pupil transfer function, $\varphi(\mathbf{x})$ is the averaged phase. Phase can be expressed with the first n terms Zernike polynomials with coefficient a_i:

$$\phi(\mathbf{x}) = \sum_{i=1}^{n} a_i Z_i(\mathbf{x}). \tag{3}$$

The other image can be similarly written as:

$$g_d(\mathbf{x}) = f(\mathbf{x}) * h_d(\mathbf{x}) + n_d(\mathbf{x}), \tag{4}$$

where the subscript d stands for phase diversity image. $h_d(\mathbf{x})$ can be written as:

$$h_d(\mathbf{x}) = \left|FT(P(\mathbf{x})\exp(i(\phi(\mathbf{x}) + \phi_d(\mathbf{x})))\right|^2, \tag{5}$$

where $\varphi_d(\mathbf{x})$ is the known defocus, $FT[]$ denotes the Fourier transform. The merit function is then obtained based on the max likelihood:

$$E = \sum_{\mathbf{x}} |g(\mathbf{x}) - f(\mathbf{x}) * h(\mathbf{x})|^2 + \left|g_d(\mathbf{x}) - f(\mathbf{x}) * h_d(\mathbf{x})\right|^2 + J(f), \tag{6}$$

where $J(f)$ stands for a regularizing term. For PD merit function we use a first order Tikhonov regularizing term [24], $J(f) = \gamma|f(\mathbf{x})|^2$. From Eq. (6), the functions can be derived in the frequency domain as follows:

$$E = \sum_{\mathbf{u}} \frac{\left|G(\mathbf{u})H(\mathbf{u}) - G_d(\mathbf{u})H_d(\mathbf{u})\right|^2}{|H(\mathbf{u})|^2 + \left|H_d(\mathbf{u})\right|^2 + \gamma}, \tag{7}$$

$$f(x) = FT^{-1}\left[\frac{H^*(\mathbf{u})G(\mathbf{u}) + H_d^*(\mathbf{u})G_d(\mathbf{u})}{|H(\mathbf{u})|^2 + \left|H_d(\mathbf{u})\right|^2 + \gamma}\right], \tag{8}$$

$\mathbf{u}$ is a two-dimensional spatial frequency, $FT^{-1}[]$ denotes the inverse Fourier transform, $G(\mathbf{u})$, $H(\mathbf{u})$, $G_d(\mathbf{u})$, $H_d(\mathbf{u})$ are the Fourier transform of $g(\mathbf{x})$, $h(\mathbf{x})$, $g_d(\mathbf{x})$, $h_d(\mathbf{x})$ respectively, and $H^*(\mathbf{u})$, $H_d{}^*(\mathbf{u})$ are the complex conjugate of $H(\mathbf{u})$, $H_d(\mathbf{u})$. Some optimization algorithms can then be used to minimize Eq. (7). The hybrid particle swarm algorithm proposed by P. G. Zhang et al. can approaches the global minimum for the PD phase retrieval with high reliability and accuracy [25], thus we will use this optimization algorithm to the PD.

3. LC AOS

The optical layout of LC AOS is shown in Fig. 2. The light from the focus of the telescope is collimated by lens 1 (L1), next a tip/tilt mirror (TTM) corrects the tip/tilt of phase distortion. Then the light is divided into two paths by long wavelength pass filter (LWPF), wavelengths shorter than 700 nm are reflected to the Shack–Hartmann wavefront sensor (SH-WFS), and the long wave band from 700 nm to 900 nm will be transmitted to wavefront-correction branch. The LC-SLMs will correct the light with the signal from the SH-WFS. Thus the LC AOS is an open-loop system and this can improve the light energy collected by the imaging camera.

The system −3 dB error rejection bandwidth is about 85 Hz. The SH-WFS has 315 effective subapertures on a 20 × 20 microlens array

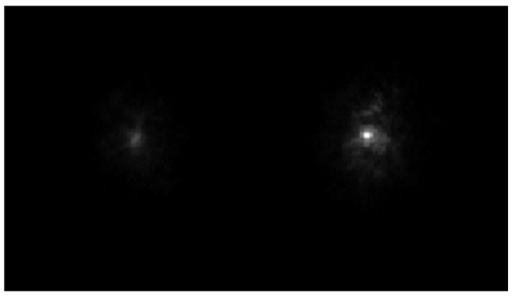

Fig. 3. One section of raw image of the star, left is image with defocus, right is image in focus.

to cover conjugate pupil image, which corresponds to 10 cm sampling over the telescope aperture. The LC corrector used here is nematic. It evolved from the LC corrector in Ref. [18]. Its response time is 0.75 ms and frame rate is 1.3 kHz. It has 256 × 256 pixels, pixel size is 2.4 μm. It has a 1 λ (λ = 780 nm) phase modulation depth. The LC-SLMs can modulate optical band from 700 nm to 900 nm, because the wavelength dependence of the modulation is less in this waveband and it can be ignored. Larger phase change can be achieved with the kinoform method. To attain enough high diffraction efficiency of LC, 1 λ phase modulation need be quantized by no less than 8 pixels. Then the maximum phase change is about 8 λ PV for defocus. The effective focal length and diameter of imaging lens L7 are 460 mm and 17 mm respectively. The imaging camera is Andor EMCCD (iXon Ultra 888) with 1024 × 1024 pixels, and the pixel size is 13 μm × 13 μm. The readout noise of the imaging camera is less than 1 e− with EM gain.

Given that LC-SLM is only useful for polarized light, two LC-SLMs are used to correct two beams whose polarization direction is perpendicular to each other. Meanwhile, it is easy to add any specific and known phase diversity in one of LC-SLMs. To separate the two corrected images, the LC-SLM with phase diversity is placed with a small tilt. Here the phase diversity is defocus with 0.8λ PV. One corrected beam and the other corrected beam with known defocus will be imaged onto two separated area on a charge coupled device (CCD). In post-processing the PD is used to retrieve residual aberration and restore image with higher resolution. Because of large computation of the PD algorithm, we get focused image and defocused image in real time but apply phase diversity for post-processing.

4. Experiments and results

The observations were conducted with 2-m telescope at Changchun Institute of Optics, Fine Mechanics and Physics, Chinese Academy of Sciences. The star was observed on March 23, 2018. Fig. 3 shows a section of one image of the star HD 29139 with size 218 × 122 pixels. There are two images of star, and the right is the image with LC AOS correction, and the left is the image with LC AOS correction and defocus.

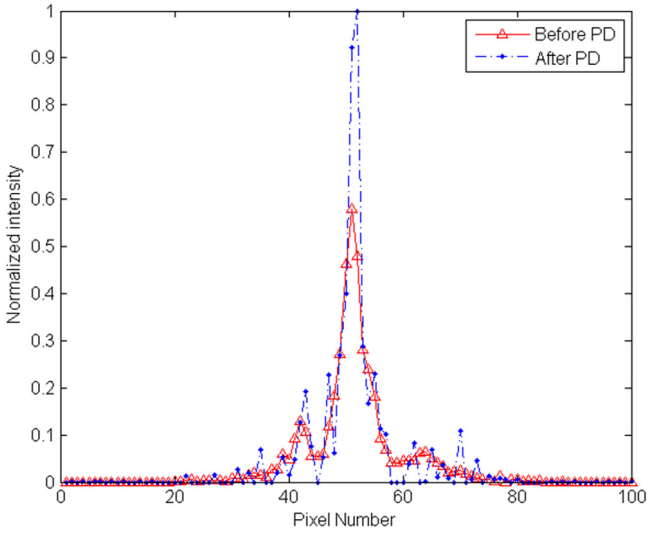

Fig. 5. Peak intensity of profile of the star before and after the PD. The red solid line with triangle is data before the PD, the blue dotted line with dot is data after the PD.

The distance between two images is about 100 pixels, so the sample number of one image for the PD is 100 × 100 pixels. In order to compensate for the effect of total intensity difference of the two images, a ratio was added to the defocused image, that is to say,

$$g_d = \frac{\sum g}{\sum g_{d0}} g_{d0}, \tag{9}$$

where g_{d0} is the original defocused image, the sum is for the total intensity of all pixels.

The two images used for the PD and deblurred image are shown as Fig. 4. Fig. 4(a) is focused image with residual aberration, Fig. 4(b) is defocused image, and Fig. 4(c) is deblurred image with the PD. The star spot is obviously smaller than Fig. 4(a). The comparison of normalized intensity of profile is shown in Fig. 5. It is indicated that the peak intensity increased by 66.7% after the PD, and the FWHM decreased from about 10 pixels to 4 pixels. Given that a pixel corresponds to 0.05″, angular resolution was improved from 0.5″ to 0.2″. Due to the diffraction limit FWHM is 2 pixels, the resolution was improved from 5 times diffraction limit to 2 times diffraction limit. It can be seen that the effect of the PD is obvious.

Table 1 gives results of eight frames. The average angular resolution is in line with Fig. 4. The RMS of reconstructed wavefronts are also presented. In fact, the wavefront and angular resolution are related to each other with SR. Thus the reconstructed wavefront by the PD can be verified with angular resolution of observed images. The SR of corresponding wavefront can be calculated approximately by Eq. (10) [26] as

$$SR \approx \exp[-(\frac{2\pi\sigma}{\lambda})^2], \tag{10}$$

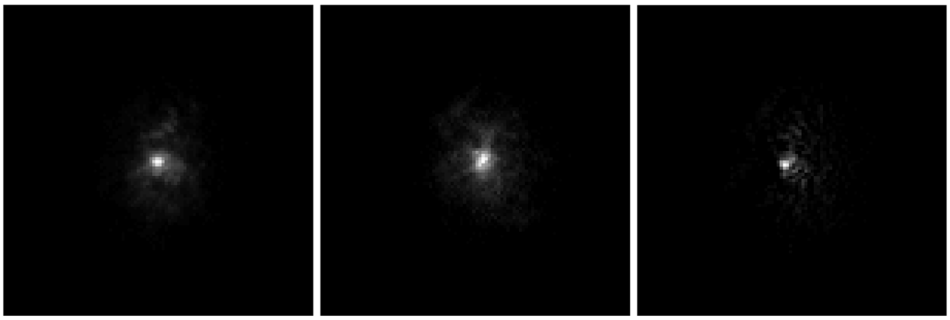

Fig. 4. Images of the star before and after the PD. (a) The focused image; (b) the defocused image; (c) the deblurred image by the PD.

Table 1
Angular resolution and restored wavefront of the star in some frames.

Frame number	Before the PD	After the PD	RMS of restored wavefront
1	0.44″	0.23″	0.1789 λ
2	0.51″	0.18″	0.4415 λ
3	0.58″	0.15″	0.2293 λ
4	0.46″	0.19″	0.1493 λ
5	0.45″	0.27″	0.2411 λ
6	0.52″	0.24″	0.3165 λ
7	0.41″	0.24″	0.2037 λ
8	0.40″	0.24″	0.3987 λ
Average	0.47″	0.22″	0.2949 λ

where σ is the RMS of the wavefront, λ is the wavelength and $\lambda = 780$ nm. The achievable angular resolution of the telescope can be expressed approximately as a function of the SR [27] as

$$\theta \approx 1.22\frac{\lambda}{D\sqrt{SR}}, \tag{11}$$

where D is the diameter of the telescope. From the average RMS of wavefronts in Table 1, the average angular resolution after AO can be calculated and is about 0.54″. This is close to the measured average value of 0.47″, which indicates that the wavefronts reconstructed from the PD are reasonable.

5. Conclusion

In this work, the PD technique was applied to LC AOS with 2-m telescope. Two LCSLMs were used for two polarized states of light, and they were also used for two channel correction of focused image and diversity image. The experimental results after the PD show that the FWHM of the star was improved from 10 pixels to 4 pixels, and the angular resolution correspondingly was improved from 0.5″ to 0.2″. The RMS of the wavefront estimated using the PD agrees with the SR of the AO corrected image. The results indicate that the PD technique can significantly improve the image resolution after LC AOS. This technique can be widely used in large aperture telescopes for astronomical observations, fluorescence microscopy, retinal adaptive optics imaging and other fields related to high resolution imaging.

Acknowledgments

This work is supported by the National Natural Science Foundation of China [No. 11774342, No. 61475152, No.11804336 and No.11704377].

References

[1] D.J. Lee, B.L. Ellerbroek, J.C. Christou, First results of the Starfire Optical Range 3.5-m telescope adaptive optics system: point spread functions and tracking performance, in: Proc. SPIE, Vol. 3353, 1998, pp. 1080–1091.
[2] C.E. Max, B.A. Macintosh, D.T. Gavel, D.S. Acton, P.L. Wizinowich, O. Lai, Neptune and Titan observed with Keck Telescope adaptive optics, Astron. Telesc. Instrum. 4007 (2000) 803–810.
[3] J.E. Roberts, R.G. Dekany, C. Baranec, A. Bouchez, M. Troy, T.N. Truong, Results from the PALM-3000 high-order adaptive optics system, in: Proc. SPIE, Vol. 8447, 2012.
[4] N.H. Turner, T.A. Ten Brummelaar, L.C. Roberts Jr., Faint companion search to O-stars using the adaptive optics system on the 3.63-m telescope on Haleakala, in: Proc. SPIE, Vol. 4839, 2003, pp. 1103–1109.
[5] N.M. Law, C.D. Mackay, J.E. Baldwin, Lucky imaging: high angular resolution imaging in the visible from the ground, Astron. Astrophys. 446 (2006) 739–745.
[6] M.G. Löfdahl, G.B. Scharmer, Wavefront sensing and image restoration from focused and defocused solar images, Astron. Astrophys. Suppl. 107 (1994) 243–264.
[7] A.W. Lohmann, G. Weigelt, B. Wirnitzer, Speckle masking in astronomy: triple correlation theory and applications, Appl. Opt. 22 (1983) 4028.
[8] R.A. Gonsalves, R. Chidlaw, Wavefront sensing by phase retrieval, in: Proc. SPIE, Vol. 207, 1979, pp. 32–39.
[9] M.G. Lofdahl, G.B. Scharmer, Application of phase-diversity to solar images, in: Proc. SPIE, Vol. 2302, 1994, pp. 254–267.
[10] J.H. Seldin, R.G. Paxman, Phase-diverse speckle reconstruction of solar data, in: Proc. SPIE, Vol. 2302, 1994, pp. 268–280.
[11] L.M. Mugnier, J.F. Sauvage, T. Fusco, A. Cornia, S. Dandy, On-line long-exposure phase diversity: a powerful tool for sensing quasi-static aberrations of extreme adaptive optics imaging systems, Opt. Express 16 (2008) 18406–18416.
[12] R.A. Gonsalves, Phase retrieval and diversity in adaptive optics, Opt. Eng. 21 (1982) 829–832.
[13] D. Wilding, P. Pozzi, O. Soloviev, G. Vdovin, M. Verhaegen, Phase diversity based object estimation in light-sheet fluorescence microscopy, OSA Technical Digest paper (2017) BoTu2A.2.
[14] R.G. Paxman, J.R. Fienup, Optical misalignment sensing and image reconstruction using phase diversity, J. Opt. Soc. Amer. A 5 (1988) 914–923.
[15] C. Robert, T. Fusco, J.F. Sauvage, L. Mugnier, Improvement of phase diversity algorithm for non-common path calibration in extreme AO context, in: Proc. SPIE, Vol. 7015, 2008.
[16] N. Védrenne, L.M. Mugnier, V. Michau, M.T. Velluet, R. Bierent, Laser beam complex amplitude measurement by phase diversity, Opt. Express 22 (2014) 4575.
[17] Z. Zhang, Z. You, D. Chu, Fundamentals of phase-only liquid crystal on silicon (LCOS) devices, Light Sci. Appl. 3 (2014) e213.
[18] Z. Cao, Q. Mu, L. Hu, D. Li, Z. Peng, Y. Liu, L. Xuan, Preliminary use of nematic liquid crystal adaptive optics with a 2.16-m reflecting telescope, Opt. Express 17 (2009) 2530.
[19] A.V. Kudryashov, J. Gonglewski, S. Browne, R. Highland, Liquid crystal phase modulator for adaptive optics. Temporal performance characterization, Opt. Commun. 141 (1997) 247–253.
[20] Q. Mu, Z. Cao, L. Hu, Y. Liu, Z. Peng, L. Yao, X. Li, Open loop adaptive optics testbed on 216 meter telescope with liquid crystal corrector, Opt. Commun. 285 (2012) 896–899.
[21] D. Dayton, J. Gonglewski, S. Restaino, J. Martin, J. Phillips, M. Hartman, P. Kervin, J. Snodgress, S. Browne, N. Heimann, Demonstration of new technology MEMS and liquid crystal adaptive optics on bright astronomical objects and satellites, Opt. Express 10 (2002) 1508–1519.
[22] Z. Cao, Q. Mu, L. Hu, Y. Liu, Z. Peng, Q. Yang, H. Meng, L. Yao, L. Xuan, Optimal energy-splitting method for an open-loop liquid crystal adaptive optics system, Opt. Express 20 (2012) 19331.
[23] Z. Xu, C. Yang, P. Zhang, X. Zhang, Z. Cao, Q. Mu, Q. Sun, L. Xuan, Visible light high-resolution imaging system for large aperture telescope by liquid crystal adaptive optics with phase diversity technique, Sci. Rep. 7 (2017) 10034.
[24] A.N. Tikhonov, On the stability of inverse problems, Dolk. Akad. Nauk SSSR 39 (1943) 176–179.
[25] P.G. Zhang, C.L. Yang, Z.H. Xu, Z.L. Cao, Q.Q. Mu, L. Xuan, Hybrid particle swarm global optimization algorithm for phase diversity phase retrieval, Opt. Express 24 (2016) 25704.
[26] V.N. Mahajan, Strehl ratio for primary aberrations in terms of their aberration variance, J. Opt. Soc. Amer. 73 (1983) 860–861.
[27] D.W. Tyler, A.E. Prochko, Adaptive optics design for the advanced electro-optical system (AEOS), Final Report (1994).